## S1 Surface anisotropy; dependence on surface type and time

Figures S1–S3 are similar to Fig. 6 in Sect. 5.2 of the paper. The wavelengths studied are 670, 463, and 380 nm instead of 772 nm as in the paper. The surface DLER is plotted versus the viewing angle θ_v for the nine land surface type regions defined in Table 2 of the paper. The coloured curves represent the average surface DLER for the calendar months indicated by the legend (February, May, August, November). The grey curves represent the spread in the surface DLER values.
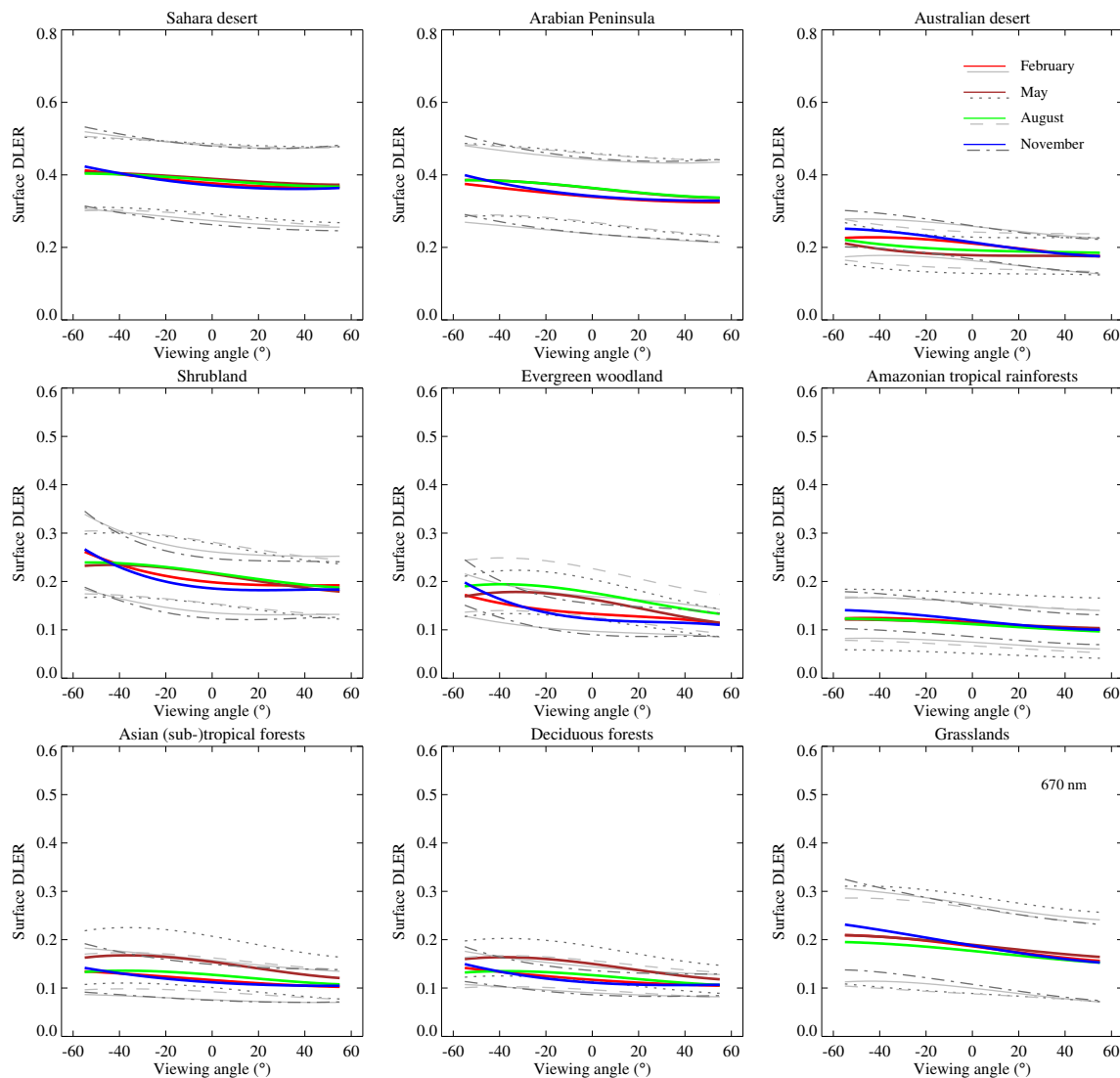
Figure S1. TROPOMI surface DLER at 670 nm as a function of the viewing angle θ_v for nine land surface type regions and four calendar months. The coloured curves represent the average surface DLER for the calendar months indicated by the legend (February, May, August, November). The grey curves represent the spread in the surface DLER values.
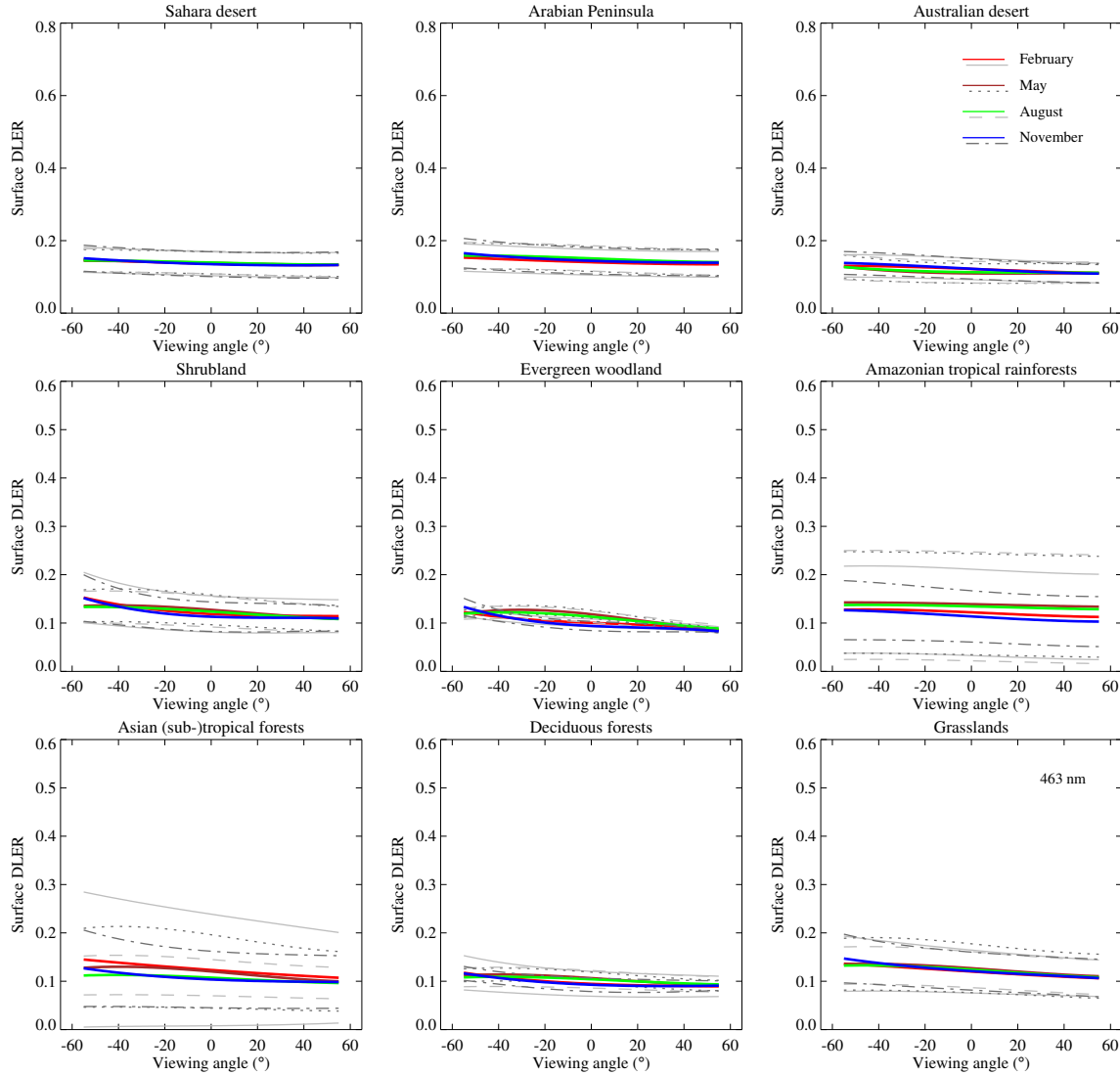
Figure S2. TROPOMI surface DLER at 463 nm as a function of the viewing angle θ_v for nine land surface type regions and four calendar months. The coloured curves represent the average surface DLER for the calendar months indicated by the legend (February, May, August, November). The grey curves represent the spread in the surface DLER values.
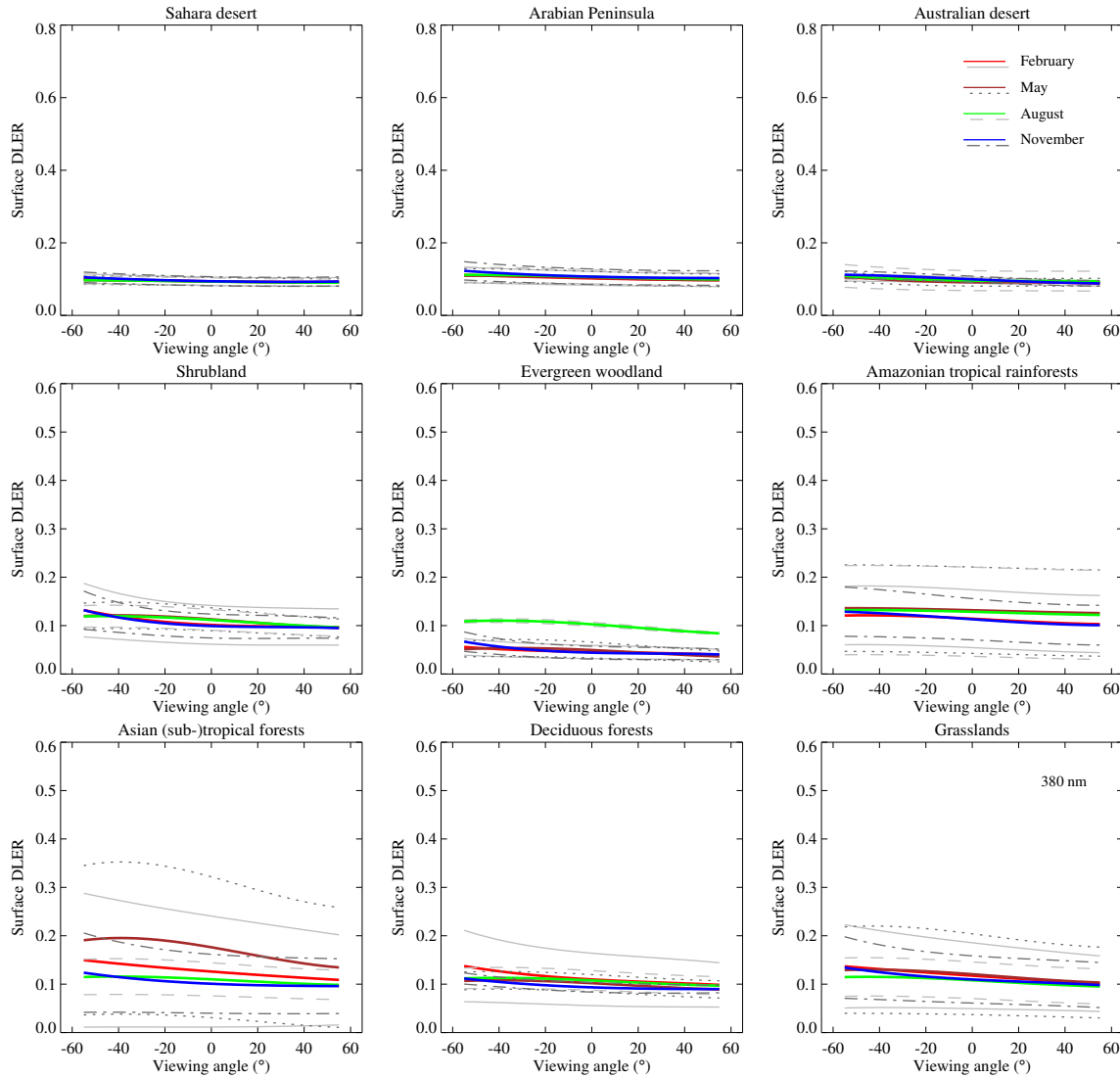
Figure S3. TROPOMI surface DLER at 380 nm as a function of the viewing angle θ_v for nine land surface type regions and four calendar months. The coloured curves represent the average surface DLER for the calendar months indicated by the legend (February, May, August, November). The grey curves represent the spread in the surface DLER values.

S2   Surface LER spectra; dependence on surface type and time

Calculations of spatial averages and standard deviations of surface LER spectra were performed for a selection of surface types. The twelve regions that were defined for this are listed in Table S1. The surface type was constrained using the Matthews land usage database (Matthews, 1983). Next to the constraint on surface type, we set constraints on latitudes and longitudes and filtered out grid cells that partly contained coastal areas. Furthermore, we checked, using NISE snow/ice information, that all land surface grid cells that were used were classified as completely snow free for all of the months, except for the "Antarctica" and "Greenland" regions. In a similar way, all ocean grid cells that were used were checked to be completely free of sea ice.

| Description	Matthews Land Type	Latitude Range	Longitude Range
Atlantic Ocean	-9999	1–59°N	20–48°W
Pacific Ocean	-9999	30°S–30°N	135–175°W
Indian Ocean	-9999	0–45°S	60–94°E
Sahara desert	30	16–27°N	12°W–15°E
Arabian Peninsula	30	15–34°N	37–61°E
Australian desert	30	15–30°S	114–145°E
Antarctica	31	73–85°S	0–45°E
Greenland	31	70–80°N	31–48°W
Amazonian tropical rainforests	1	15°S–10°N	40–85°W
Asian (sub-)tropical forests	2,5,7,9	10–35°N	70–125°E
Deciduous forests	9–11	0–40°N	–
Grasslands	23–28	35°S–35°N	–

Table S1. Definition of the surface type tegions studied in Fig. S4. The symbol – indicates that no constraint was set on the longitude.

In Fig. S4 we present the results that were based on the TROPOMI surface LER database. Each of the twelve windows presents the average surface LER as well as the standard deviation as a function of wavelength, for the months February, May, August, and November. The coloured curves refer to the surface LER averages, the gray curves to the standard deviations (see both legends in Fig. S4).

## S3   Validation using heritage databases as reference

S3.1   Histograms

Figures S5–S7 present examples of histograms of the differences between the TROPOMI surface LER and the surface LER from SCIAMACHY (at 380 nm), OMI (at 494 nm), and GOME-2 (at 494 nm), respectively, for each of the twelve calendar months. Note that the LER difference on the horizontal axis was multiplied by 100. The black histograms are determined from all grid cells between 60°S and 60°. From these, blue histograms are created from the grid cells over the ocean and green histograms from the grid cells over land. Differences in spatial resolution between the LER databases are handled by performing binning of the smaller grid cells to the size of the larger grid cells. The mean values of the distributions are represented by the dashed vertical lines, the modes of the distributions are given by the dotted vertical lines.
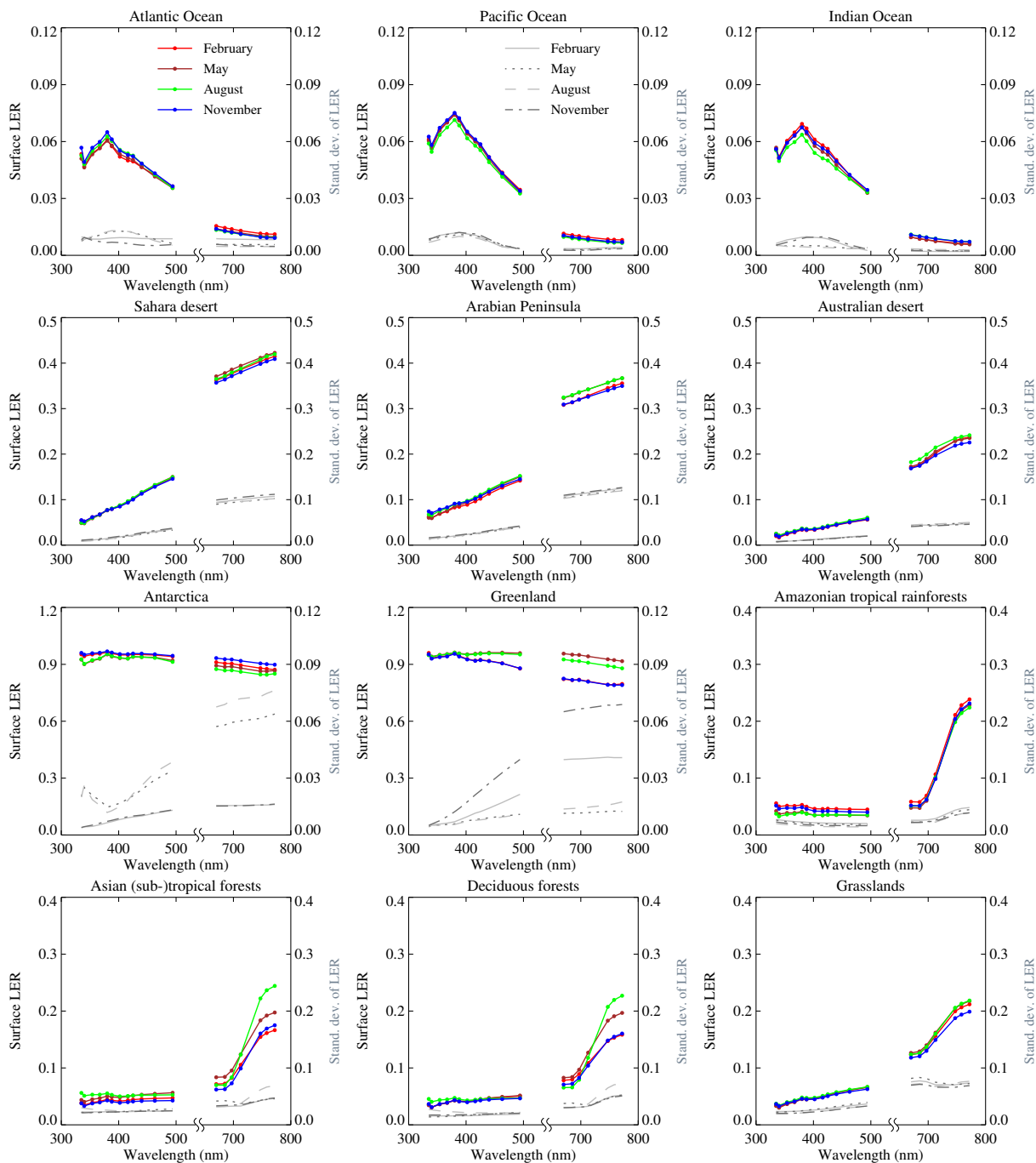
Figure S4. TROPOMI surface LER spectra, calculated for the surface type regions defined in Table S1, and presented for the months February (red), May (brown), August (green), and November (blue). The additional gray spectra represent the standard deviation in the surface LER spectra contained in the surface type regions. The 2314-nm wavelength band was left out for clarity.

TROPOMI MIN-LER (380 nm) versus SCIAMACHY MIN-LER (380 nm)
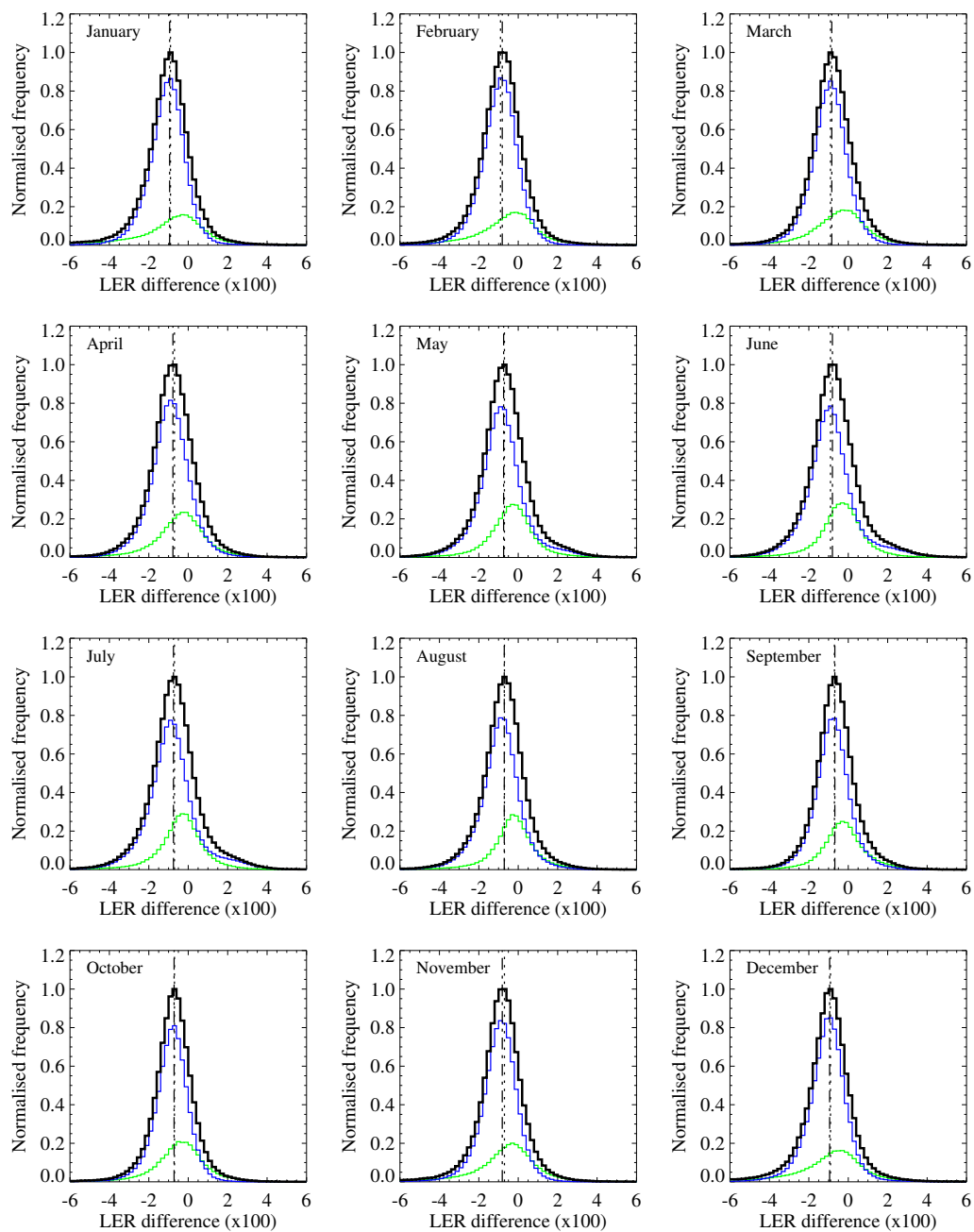
Figure S5. Histograms of the difference between the surface LER from TROPOMI and that of SCIAMACHY for 380 nm and for all calendar months. The black histograms are made up of all grid cells between $60°S$ and $60°$. The blue histograms are determined from the subset of grid cells over the ocean and the green histograms are determined from the subset of grid cells over land.

TROPOMI MIN-LER (494 nm) versus OMI MIN-LER (494 nm)
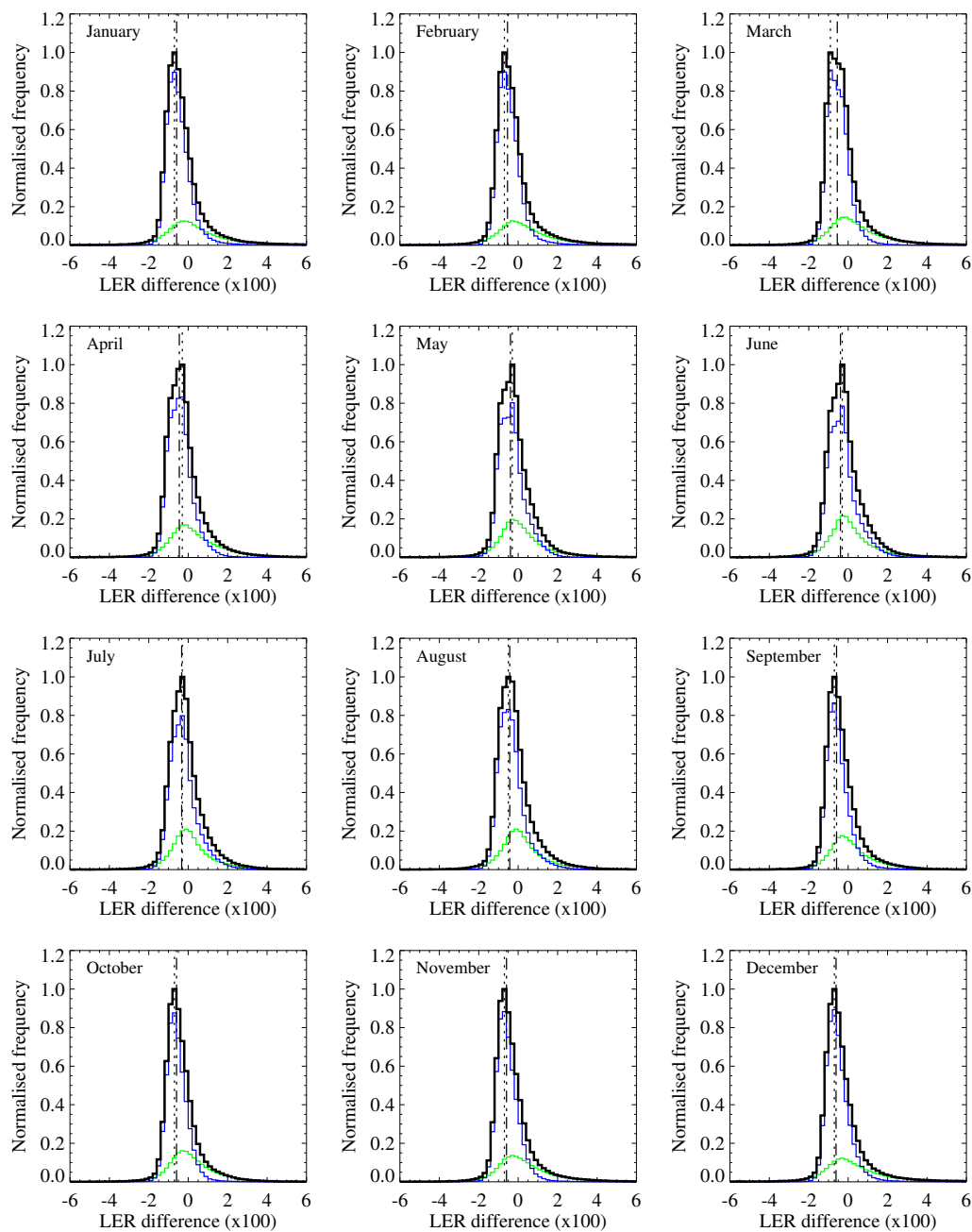
Figure S6. Histograms of the difference between the surface LER from TROPOMI and that of OMI for 494 nm and for all calendar months. The black histograms are made up of all grid cells between 60°S and 60°. The blue histograms are determined from the subset of grid cells over the ocean and the green histograms are determined from the subset of grid cells over land.

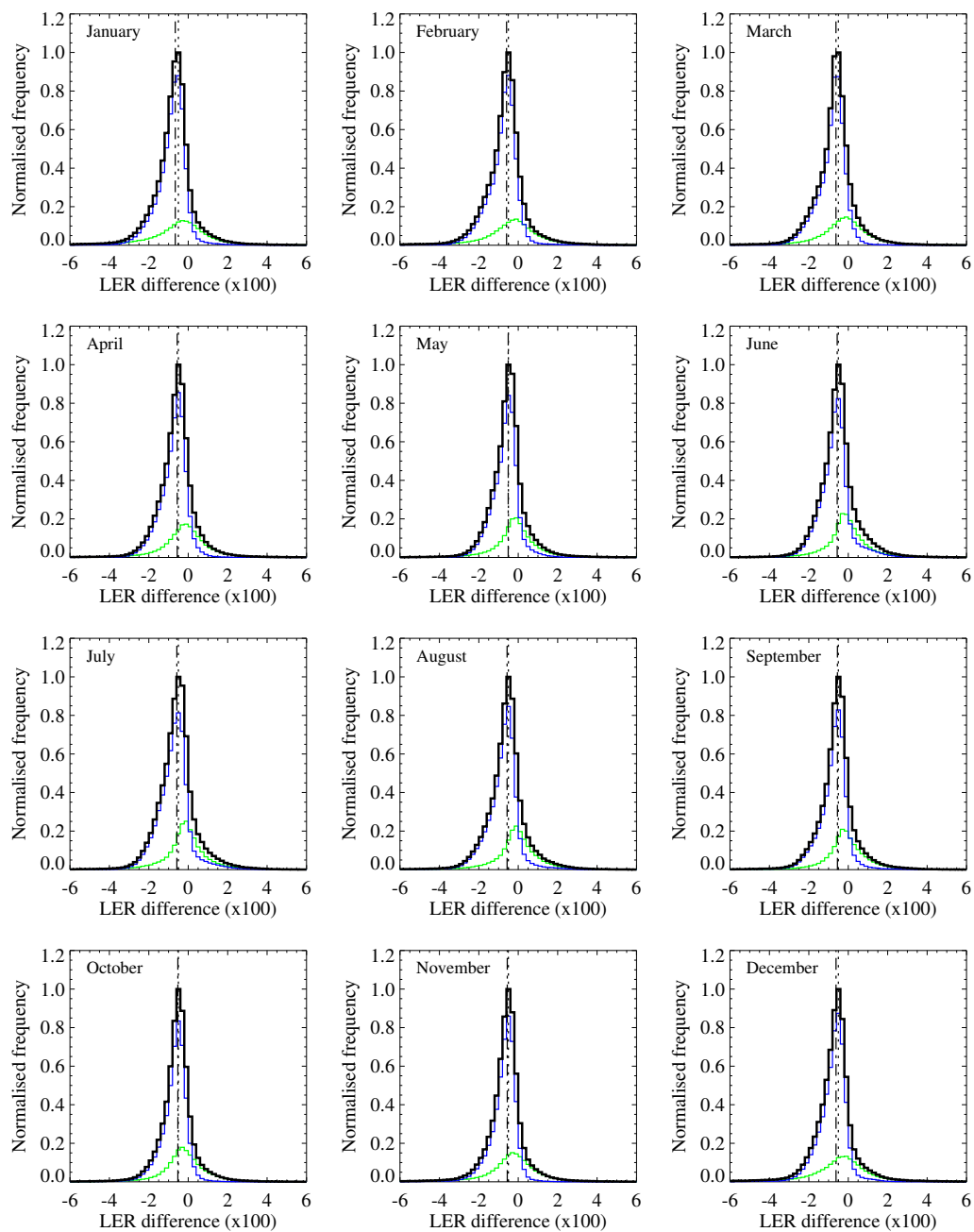TROPOMI MIN-LER (494 nm) versus GOME-2ABC MIN-LER (494 nm)

Figure S7. Histograms of the difference between the surface LER from TROPOMI and that of GOME-2 for 494 nm and for all calendar months. The black histograms are made up of all grid cells between 60°S and 60°. The blue histograms are determined from the subset of grid cells over the ocean and the green histograms are determined from the subset of grid cells over land.

S3.2 Accuracy tables

Tables S2–S4 contain the validation results from the comparisons in which the TROPOMI surface LER database was compared to the heritage surface LER databases based on SCIAMACHY, OMI and GOME-2, respectively. The tables present the mean surface LER difference, multiplied by 100 and based only on the grid cells with latitude between 60°S and 60°N, and the FWHM of the distributions, also multiplied by 100. The results are available for each mutual wavelength band and for each of the twelve calendar months.

TROPOMI versus OMI (MIN-LER)

Mean surface LER difference (×100)

λ (nm)	JAN	FEB	MAR	APR	MAY	JUN	JUL	AUG	SEP	OCT	NOV	DEC
328	-1.20	-1.31	-1.27	-1.22	-1.19	-1.27	-1.16	-1.10	-1.04	-0.90	-0.91	-1.11
335	-1.31	-1.36	-1.36	-1.36	-1.41	-1.52	-1.42	-1.37	-1.26	-1.13	-1.09	-1.25
342	-1.82	-1.85	-1.87	-1.89	-1.95	-2.08	-1.97	-1.91	-1.80	-1.66	-1.63	-1.78
354	-1.31	-1.33	-1.35	-1.35	-1.41	-1.53	-1.42	-1.35	-1.28	-1.15	-1.12	-1.27
367	-0.96	-0.98	-0.98	-0.96	-1.02	-1.14	-1.05	-0.97	-0.94	-0.86	-0.86	-0.97
380	-0.53	-0.55	-0.55	-0.48	-0.49	-0.56	-0.48	-0.49	-0.52	-0.48	-0.48	-0.55
388	-0.89	-0.89	-0.89	-0.83	-0.84	-0.92	-0.83	-0.82	-0.86	-0.83	-0.83	-0.92
416	-1.00	-0.96	-0.94	-0.86	-0.86	-0.93	-0.84	-0.86	-0.96	-0.95	-0.97	-1.04
425	-0.93	-0.89	-0.87	-0.78	-0.75	-0.81	-0.72	-0.77	-0.89	-0.89	-0.91	-0.97
440	-0.83	-0.79	-0.78	-0.68	-0.64	-0.68	-0.60	-0.67	-0.80	-0.79	-0.81	-0.86
463	-0.77	-0.72	-0.72	-0.62	-0.56	-0.58	-0.51	-0.60	-0.75	-0.76	-0.77	-0.80
494	-0.59	-0.54	-0.55	-0.45	-0.39	-0.39	-0.33	-0.43	-0.59	-0.59	-0.59	-0.61

FWHM of distribution (×100)

λ (nm)	JAN	FEB	MAR	APR	MAY	JUN	JUL	AUG	SEP	OCT	NOV	DEC
328	1.89	1.94	1.94	1.93	1.85	1.92	1.85	1.91	1.78	1.84	1.92	1.84
335	1.81	1.83	1.84	1.83	1.80	1.82	1.76	1.83	1.75	1.79	1.83	1.79
342	1.83	1.84	1.88	1.92	1.92	1.93	1.86	1.88	1.76	1.79	1.82	1.79
354	1.82	1.87	1.90	1.93	1.90	1.89	1.82	1.84	1.74	1.77	1.79	1.79
367	1.74	1.76	1.82	1.83	1.76	1.76	1.70	1.79	1.65	1.67	1.71	1.71
380	1.68	1.71	1.78	1.83	1.73	1.69	1.64	1.74	1.62	1.65	1.70	1.67
388	1.68	1.72	1.79	1.82	1.72	1.69	1.63	1.73	1.63	1.67	1.72	1.67
416	1.58	1.62	1.68	1.72	1.64	1.63	1.56	1.65	1.56	1.61	1.65	1.59
425	1.54	1.57	1.63	1.69	1.63	1.61	1.55	1.62	1.51	1.55	1.61	1.54
440	1.47	1.49	1.55	1.63	1.59	1.59	1.53	1.57	1.45	1.47	1.52	1.46
463	1.34	1.36	1.41	1.51	1.52	1.54	1.48	1.48	1.34	1.33	1.36	1.32
494	1.30	1.28	1.31	1.42	1.45	1.50	1.44	1.42	1.26	1.23	1.25	1.24

Table S2. Mean difference in the surface LER of the TROPOMI and OMI surface LER databases. The FWHM of the distribution is also given. The numbers have been multiplied by 100.

TROPOMI versus SCIAMACHY (MIN-LER)

Mean surface LER difference ($\times 100$)

λ (nm)	JAN	FEB	MAR	APR	MAY	JUN	JUL	AUG	SEP	OCT	NOV	DEC
328	-2.45	-2.14	-2.14	-2.11	-1.96	-2.02	-1.96	-1.81	-1.74	-1.84	-2.14	-2.45
335	-2.21	-1.94	-1.96	-1.95	-1.83	-1.86	-1.82	-1.73	-1.65	-1.75	-1.98	-2.23
340	-2.58	-2.33	-2.38	-2.38	-2.32	-2.37	-2.31	-2.20	-2.08	-2.19	-2.41	-2.63
354	-2.15	-1.96	-2.01	-1.99	-1.91	-1.98	-1.92	-1.86	-1.78	-1.86	-2.00	-2.16
367	-1.33	-1.17	-1.19	-1.13	-1.05	-1.10	-1.04	-1.03	-1.01	-1.06	-1.18	-1.33
380	-0.94	-0.81	-0.84	-0.78	-0.74	-0.80	-0.75	-0.71	-0.68	-0.72	-0.81	-0.95
388	-0.83	-0.71	-0.74	-0.69	-0.66	-0.72	-0.67	-0.61	-0.59	-0.64	-0.72	-0.85
425	-0.72	-0.61	-0.63	-0.58	-0.54	-0.64	-0.58	-0.51	-0.49	-0.53	-0.60	-0.71
440	-0.56	-0.46	-0.49	-0.46	-0.43	-0.53	-0.48	-0.41	-0.38	-0.41	-0.46	-0.55
463	-0.41	-0.32	-0.37	-0.34	-0.33	-0.43	-0.37	-0.31	-0.28	-0.30	-0.34	-0.41
494	-0.18	-0.11	-0.16	-0.14	-0.14	-0.22	-0.17	-0.12	-0.09	-0.11	-0.14	-0.19
670	0.16	0.20	0.14	0.15	0.14	0.08	0.11	0.14	0.16	0.16	0.16	0.15
685	0.11	0.15	0.10	0.10	0.10	0.04	0.07	0.10	0.11	0.11	0.11	0.11
697	0.08	0.11	0.06	0.06	0.06	0.00	0.03	0.06	0.07	0.06	0.07	0.07
712	0.04	0.08	0.02	0.02	0.02	-0.03	-0.01	0.02	0.02	0.01	0.02	0.02
758	-0.02	0.01	-0.04	-0.03	-0.04	-0.09	-0.07	-0.04	-0.05	-0.05	-0.04	-0.04
772	-0.01	0.02	-0.03	-0.02	-0.02	-0.08	-0.06	-0.03	-0.03	-0.04	-0.03	-0.03
2314	0.01	0.02	0.01	0.02	0.09	0.04	-0.04	0.08	0.09	-0.03	-0.03	-0.02

FWHM of distribution ($\times 100$)

λ (nm)	JAN	FEB	MAR	APR	MAY	JUN	JUL	AUG	SEP	OCT	NOV	DEC
328	2.76	2.85	2.85	3.11	3.33	3.51	3.40	3.11	2.92	2.65	2.69	2.75
335	2.44	2.48	2.46	2.73	2.97	3.16	3.04	2.70	2.52	2.32	2.39	2.47
340	2.48	2.50	2.51	2.79	2.92	3.05	2.98	2.75	2.54	2.32	2.43	2.49
354	2.41	2.46	2.50	2.77	2.89	3.03	2.98	2.68	2.44	2.25	2.39	2.43
367	2.15	2.21	2.22	2.39	2.49	2.58	2.51	2.25	2.07	1.99	2.10	2.13
380	2.13	2.16	2.15	2.25	2.24	2.32	2.28	2.12	1.98	1.93	2.05	2.08
388	2.05	2.07	2.06	2.14	2.12	2.20	2.16	2.00	1.88	1.84	1.96	2.00
425	1.85	1.83	1.78	1.81	1.76	1.80	1.82	1.75	1.68	1.64	1.77	1.81
440	1.72	1.71	1.66	1.70	1.65	1.67	1.72	1.65	1.57	1.53	1.65	1.69
463	1.51	1.51	1.46	1.52	1.50	1.52	1.57	1.48	1.40	1.38	1.47	1.50
494	1.30	1.30	1.25	1.31	1.34	1.33	1.38	1.28	1.22	1.22	1.29	1.31
670	0.89	0.90	0.86	0.93	0.99	0.98	1.07	0.91	0.90	0.92	0.99	0.97
685	0.87	0.89	0.84	0.91	0.97	0.97	1.05	0.89	0.89	0.91	0.97	0.95
697	0.87	0.88	0.84	0.92	0.99	0.98	1.05	0.89	0.89	0.92	0.98	0.96
712	0.86	0.89	0.84	0.92	1.03	1.02	1.08	0.90	0.92	0.93	0.98	0.96
758	0.82	0.86	0.81	0.89	0.96	0.95	1.00	0.85	0.86	0.88	0.92	0.91
772	0.81	0.85	0.80	0.88	0.94	0.94	0.98	0.84	0.85	0.87	0.90	0.90
2314	0.69	0.64	0.63	0.65	0.47	0.67	1.01	0.48	0.45	0.77	0.83	0.83

Table S3. Mean difference in the surface LER of the TROPOMI and SCIAMACHY surface LER databases. The FWHM of the distribution is also given. The numbers have been multiplied by 100.

TROPOMI versus GOME-2 (MIN-LER)

Mean surface LER difference (×100)

λ (nm)	JAN	FEB	MAR	APR	MAY	JUN	JUL	AUG	SEP	OCT	NOV	DEC
328	-5.27	-5.20	-4.97	-4.31	-3.75	-3.76	-4.02	-4.32	-4.44	-4.51	-4.64	-4.99
335	-4.26	-4.21	-4.09	-3.56	-3.18	-3.19	-3.38	-3.56	-3.67	-3.71	-3.77	-4.07
340	-4.13	-4.10	-4.03	-3.59	-3.25	-3.26	-3.44	-3.60	-3.69	-3.69	-3.75	-3.99
354	-3.45	-3.42	-3.36	-3.03	-2.77	-2.80	-2.95	-3.05	-3.08	-3.03	-3.09	-3.30
367	-2.67	-2.65	-2.61	-2.37	-2.16	-2.20	-2.32	-2.39	-2.41	-2.34	-2.39	-2.56
380	-2.31	-2.28	-2.28	-2.09	-1.93	-1.99	-2.09	-2.12	-2.11	-2.01	-2.05	-2.20
388	-2.26	-2.22	-2.24	-2.06	-1.94	-2.00	-2.07	-2.07	-2.06	-1.97	-2.02	-2.17
416	-1.39	-1.32	-1.32	-1.16	-1.07	-1.13	-1.18	-1.15	-1.17	-1.14	-1.19	-1.32
425	-1.31	-1.24	-1.23	-1.10	-0.99	-1.05	-1.10	-1.10	-1.11	-1.07	-1.12	-1.23
440	-1.09	-1.02	-1.04	-0.91	-0.83	-0.89	-0.92	-0.92	-0.92	-0.88	-0.93	-1.02
463	-0.97	-0.89	-0.91	-0.81	-0.75	-0.80	-0.83	-0.82	-0.81	-0.79	-0.82	-0.91
494	-0.66	-0.59	-0.62	-0.56	-0.51	-0.56	-0.58	-0.57	-0.55	-0.53	-0.56	-0.62
670	-0.14	-0.11	-0.15	-0.13	-0.10	-0.15	-0.17	-0.16	-0.13	-0.10	-0.12	-0.14
685	-0.15	-0.13	-0.17	-0.14	-0.12	-0.17	-0.19	-0.18	-0.15	-0.12	-0.14	-0.16
697	-0.19	-0.16	-0.20	-0.18	-0.16	-0.21	-0.22	-0.21	-0.18	-0.16	-0.18	-0.19
712	-0.21	-0.18	-0.22	-0.20	-0.18	-0.22	-0.24	-0.23	-0.21	-0.20	-0.21	-0.22
747	-0.25	-0.23	-0.27	-0.25	-0.23	-0.28	-0.29	-0.28	-0.26	-0.25	-0.27	-0.26
758	-0.23	-0.22	-0.26	-0.24	-0.22	-0.27	-0.28	-0.27	-0.26	-0.24	-0.26	-0.25
772	-0.25	-0.24	-0.27	-0.25	-0.24	-0.28	-0.30	-0.29	-0.27	-0.26	-0.28	-0.27

FWHM of distribution (×100)

λ (nm)	JAN	FEB	MAR	APR	MAY	JUN	JUL	AUG	SEP	OCT	NOV	DEC
328	2.40	2.29	2.28	2.34	2.61	2.71	2.64	2.57	2.46	2.22	2.44	2.45
335	2.10	2.01	1.99	1.97	2.15	2.34	2.30	2.22	2.09	1.93	2.11	2.15
340	2.00	1.95	1.93	1.82	1.93	2.13	2.12	2.02	1.95	1.86	2.04	2.07
354	2.00	2.00	2.00	1.82	1.77	1.92	1.98	1.97	1.94	1.92	2.01	2.04
367	1.90	1.94	1.94	1.78	1.65	1.77	1.88	1.91	1.87	1.86	1.91	1.94
380	1.96	2.00	2.03	1.94	1.79	1.92	2.08	2.11	1.99	1.91	1.92	1.95
388	1.91	1.96	1.96	1.89	1.76	1.88	2.02	2.02	1.91	1.84	1.85	1.91
416	1.71	1.74	1.74	1.65	1.48	1.58	1.73	1.68	1.54	1.48	1.52	1.65
425	1.71	1.74	1.72	1.64	1.48	1.58	1.72	1.68	1.52	1.46	1.50	1.65
440	1.65	1.66	1.65	1.59	1.45	1.56	1.69	1.63	1.46	1.39	1.43	1.59
463	1.53	1.54	1.51	1.49	1.40	1.51	1.63	1.53	1.36	1.30	1.33	1.48
494	1.35	1.37	1.33	1.36	1.29	1.40	1.49	1.37	1.24	1.17	1.17	1.32
670	0.85	0.89	0.81	0.87	0.85	0.89	1.01	0.85	0.84	0.86	0.85	0.89
685	0.83	0.87	0.80	0.85	0.83	0.87	0.98	0.83	0.83	0.85	0.84	0.88
697	0.83	0.87	0.81	0.85	0.84	0.86	0.96	0.83	0.84	0.86	0.85	0.88
712	0.83	0.88	0.82	0.87	0.87	0.89	0.97	0.86	0.87	0.89	0.87	0.90
747	0.84	0.91	0.86	0.88	0.87	0.88	0.95	0.86	0.87	0.89	0.88	0.91
758	0.83	0.90	0.85	0.88	0.85	0.86	0.92	0.85	0.87	0.89	0.87	0.90
772	0.83	0.90	0.85	0.87	0.86	0.86	0.93	0.85	0.87	0.89	0.88	0.91

Table S4. Mean difference in the surface LER of the TROPOMI and GOME-2 surface LER databases. The FWHM of the distribution is also given. The numbers have been multiplied by 100.

S4   DLER versus MODIS BRDF

S4.1   Scatter plots

Figures S8–S17 present the comparisons between TROPOMI surface LER/DLER and MODIS surface BRDF in the form of
scatter plots for all twelve calendar months for the following case studies:

1. Libyan desert (25–29°N ; 23–27°E ; 670 nm)

2. Sahara desert (16–20°N ; 11–15°E ; 670 nm)

3. North America (32–40°N ; 85–100°W ; 670 nm)

4. Northern Africa (16–29°N ; 8°W–30°E ; 670 nm)

5. Equatorial Africa (1–7°S ; 17–29°E ; 772 nm)

Figures S8–S15 provide the results which were used to generate Fig. S18.

S4.2   Fit results

In Fig. S18 we analyse the temporal behaviour of the fit results for four of the eight regions introduced and studied in Sect. 6.2
of the paper, as clarified by the legend. Figures S8–S15 present the individual scatter plots which led to Fig. S18 for all months
for the four geographical regions studied in Fig. S18. The dashed lines in Fig. S18 refer to the LER–BRDF comparisons, the
solid lines refer to the DLER–BRDF comparisons. The left window shows that the correlation between LER and BRDF is
already good, but that the correlation between DLER and BRDF is much higher. Also, the lines are more flat, indicating a
lower dependence on calendar month. The right window shows that σ, the standard deviation of the data points with respect to
the linear fit, is lower for the DLER–BRDF comparisons than for the LER–BRDF comparisons, for all months. For the other
four regions the results are not shown, because the anisotropy of the surface is low at 670 nm, while for the Greenland region
this is because not all months are available. However, also for these four regions the DLER–BRDF comparison shows better
results than the LER–BRDF comparison in all situations.
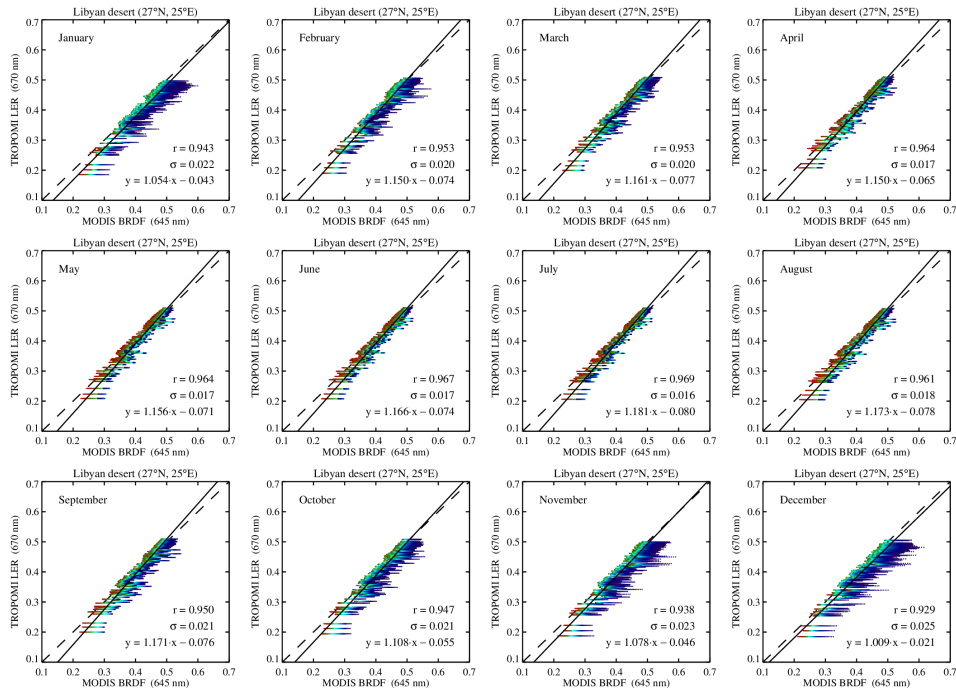
Figure S8. TROPOMI surface LER at 670 nm versus MODIS surface BRDF for the Libyan desert.
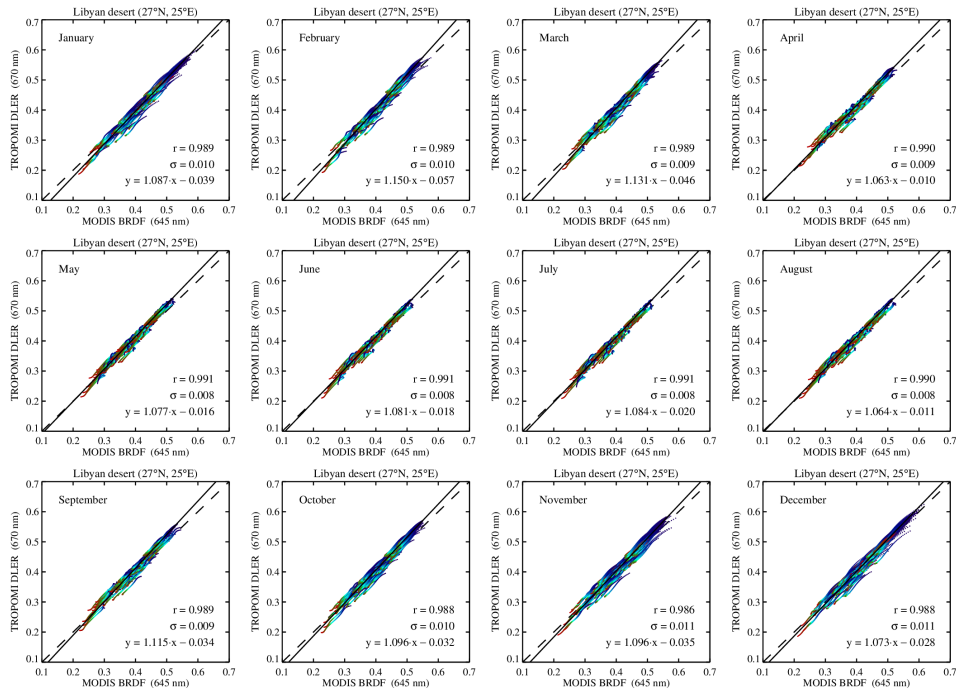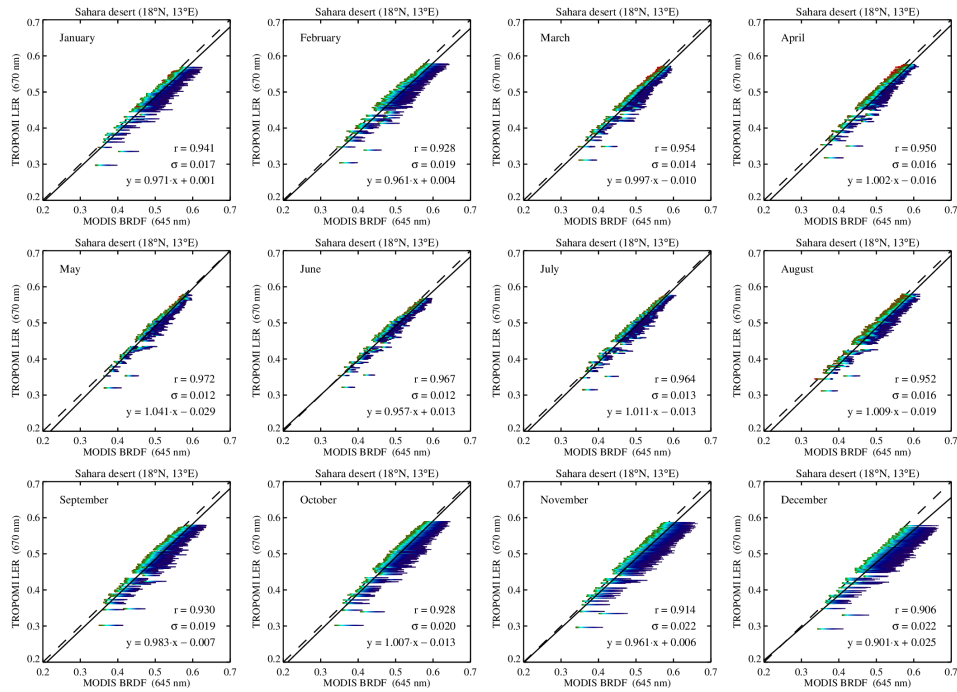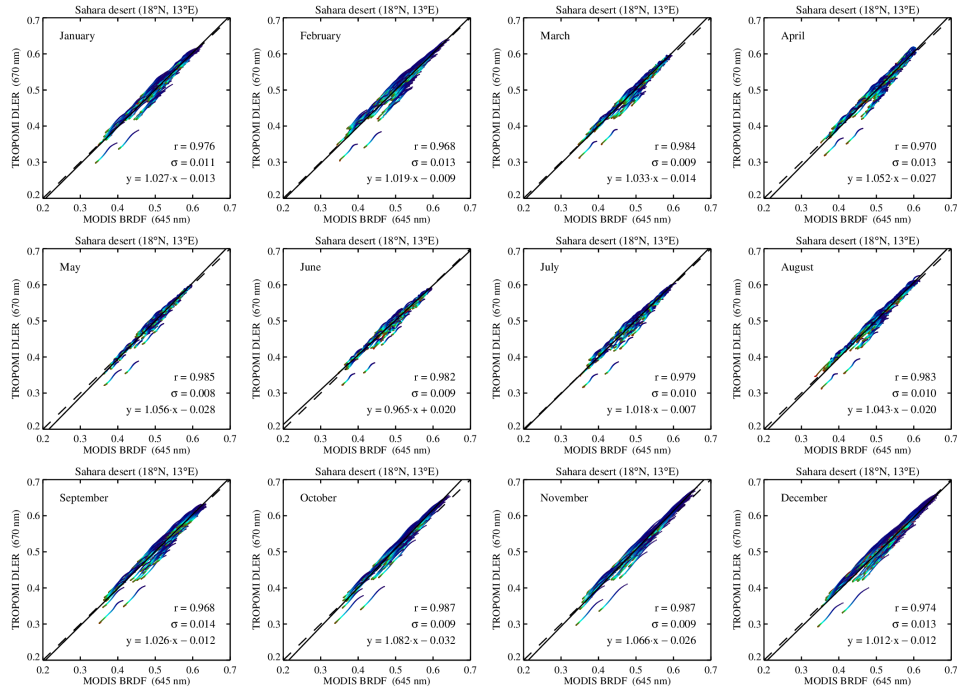

Figure S9. TROPOMI surface DLER at 670 nm versus MODIS surface BRDF for the Libyan desert.

Figure S10. TROPOMI surface LER at 670 nm versus MODIS surface BRDF for the Sahara desert.

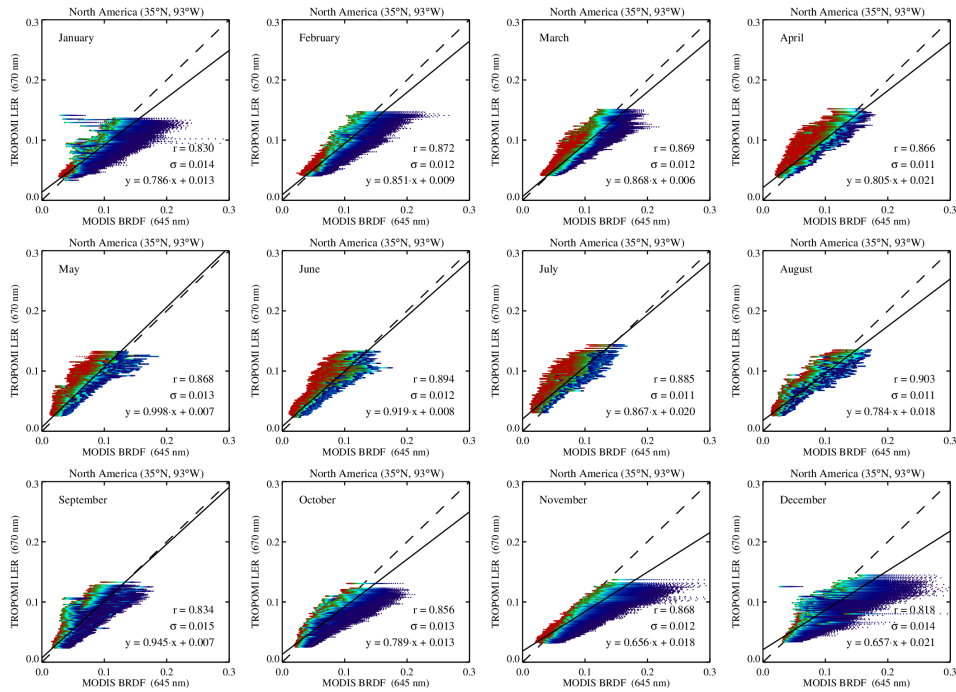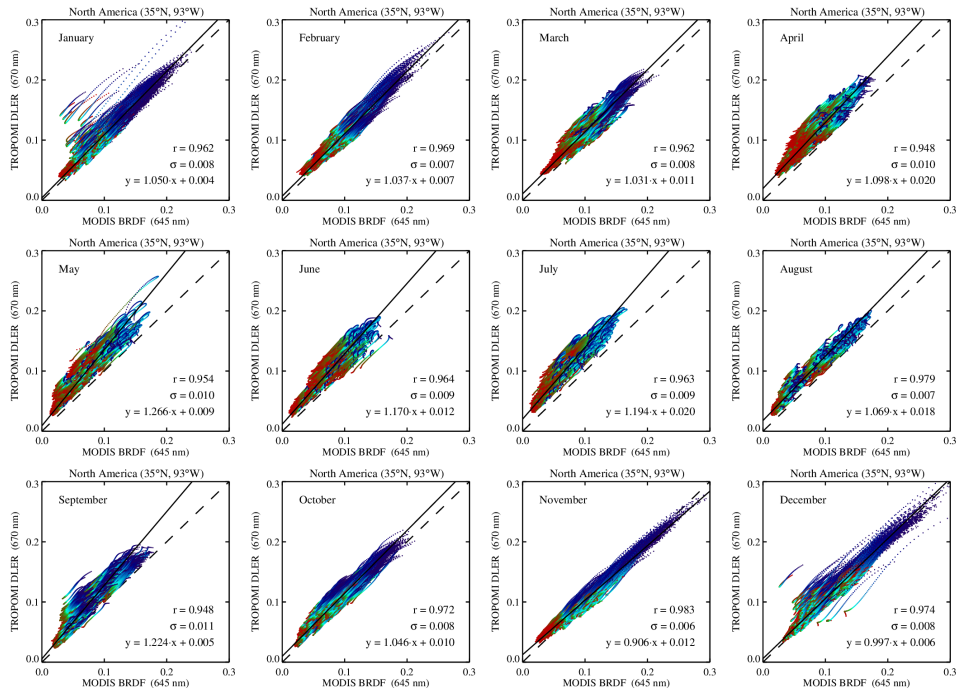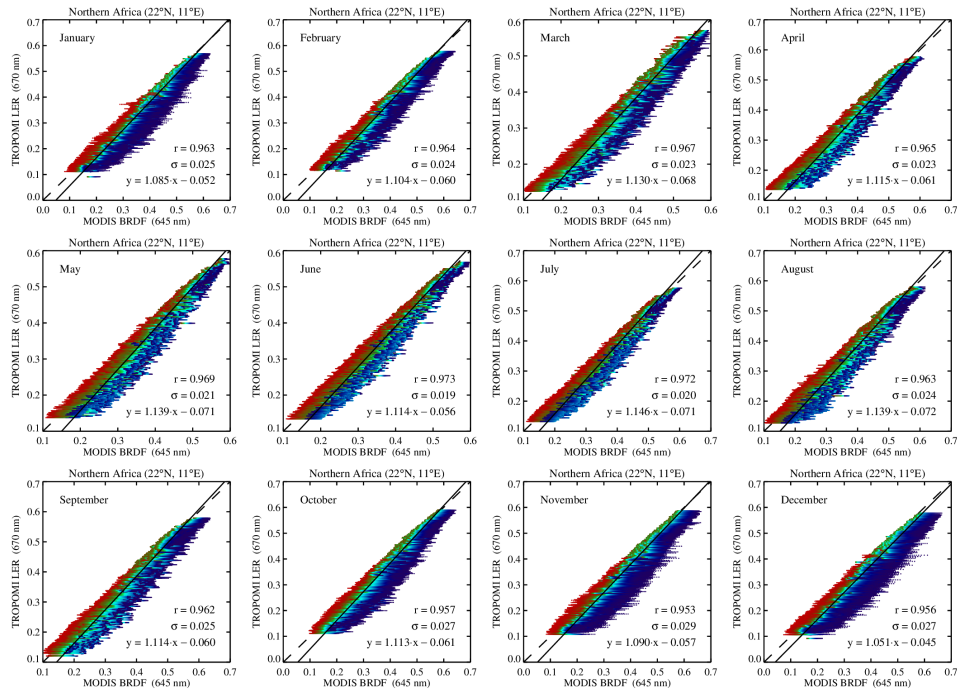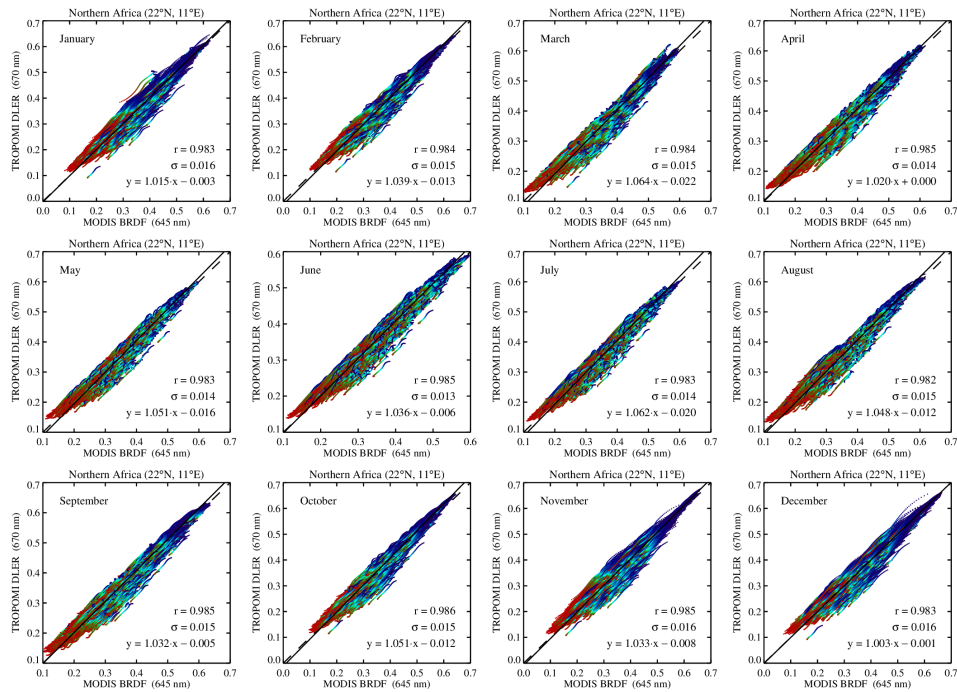**Figure S11.** TROPOMI surface DLER at 670 nm versus MODIS surface BRDF for the Sahara desert.

Figure S12. TROPOMI surface LER at 670 nm versus MODIS surface BRDF for North America.

Figure S13. TROPOMI surface DLER at 670 nm versus MODIS surface BRDF for North America.
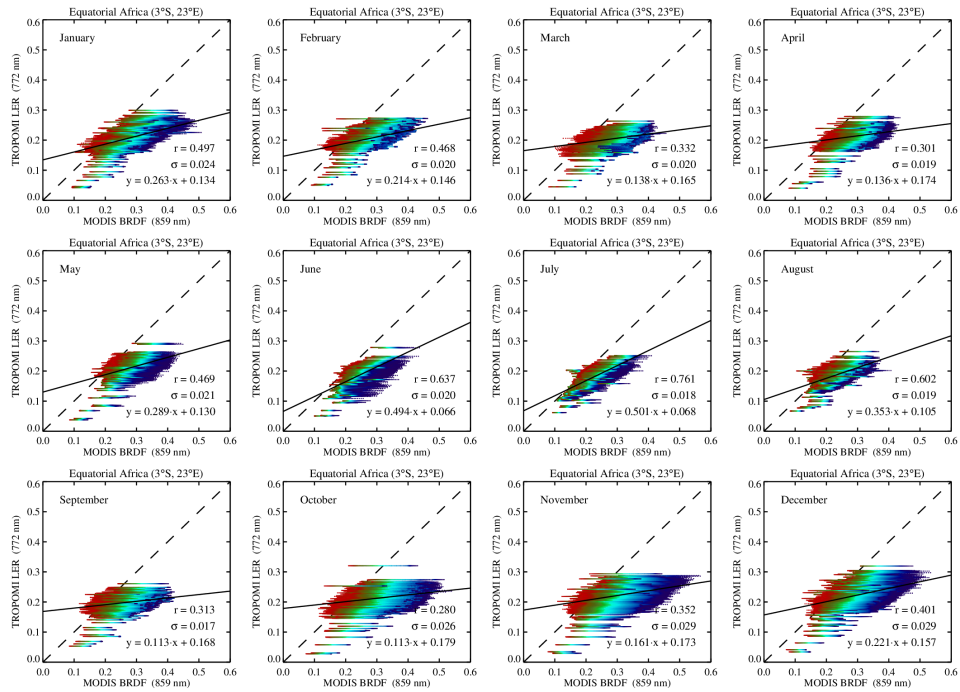
Figure S14. TROPOMI surface LER at 670 nm versus MODIS surface BRDF for Northern Africa.

Figure S15. TROPOMI surface DLER at 670 nm versus MODIS surface BRDF for Northern Africa.

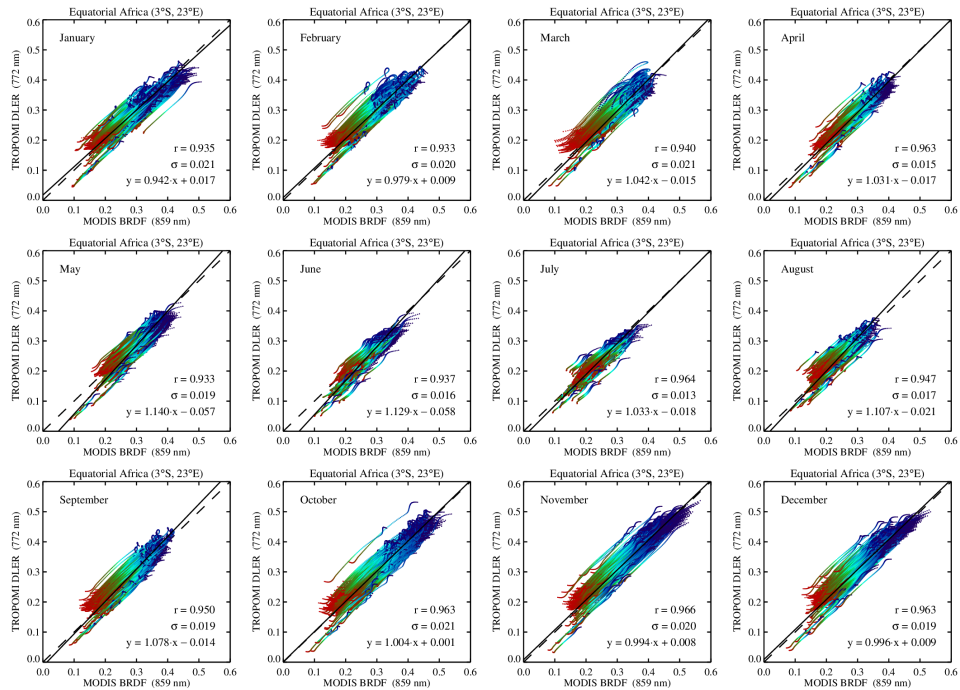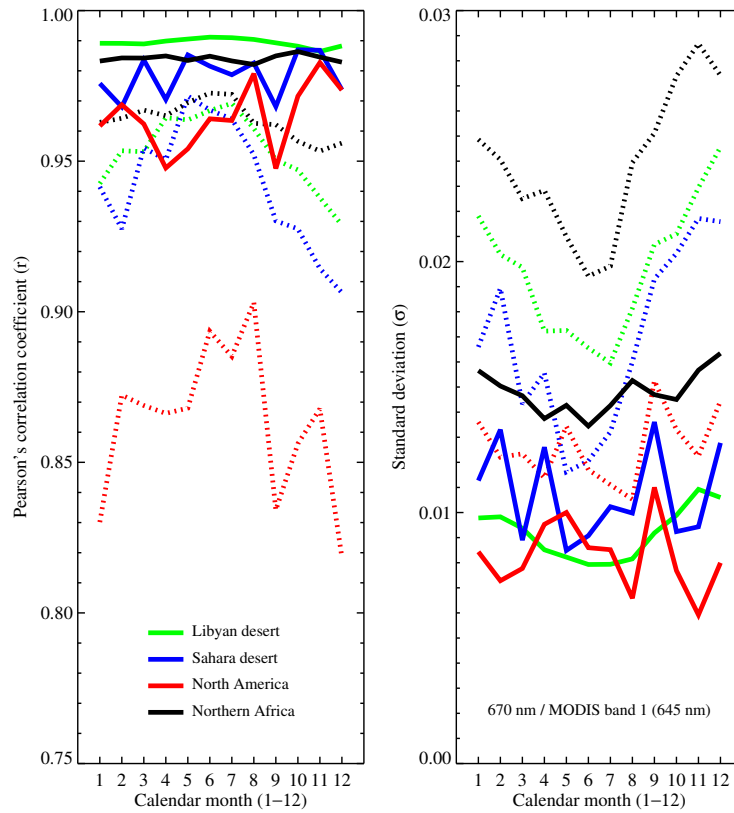**Figure S16.** TROPOMI surface LER at 772 nm versus MODIS surface BRDF for Equatorial Africa.

Figure S17. TROPOMI surface DLER at 772 nm versus MODIS surface BRDF for Equatorial Africa.

Figure S18. Fit results of the linear fits to the data points as presented in Fig. 11 of the paper. Left: Pearson's correlation coefficient r as a function of calendar month for the four indicated geographical regions. The fit results are provided for the TROPOMI surface LER as a basis (dashed lines) and for the DLER as a basis (solid lines). Right: Standard deviation σ as a function of calendar month. In all presented situations the DLER performs better than the LER.

Appendix A: Kernels for the Ross–Li BRDF model

This appendix lists the equations needed to calculate the kernels that make up the Ross–Li BRDF model of surface reflectance. Proper derivations of the Ross–Thick and Li–Sparse kernels can be found in Wanner et al. (1995).

A1 Ross–Thick volumetric kernel

The Ross–Thick volumetric scattering kernel is defined in the following way (Roujean et al., 1992):

$$K_{\text{vol}} = \frac{(\pi/2 - \xi)\cos\xi + \sin\xi}{\cos\theta + \cos\theta_0} - \frac{\pi}{4} \, . \tag{A1}$$

In Eq. (A1), θ refers to the viewing zenith angle and θ_0 to the solar zenith angle. The angle ξ is defined according to

$$\cos\xi = \cos\theta\cos\theta_0 + \sin\theta\sin\theta_0\cos(\psi - \psi') \, , \tag{A2}$$

where ψ and ψ' are the viewing and solar azimuth angles following the definition in Strahler et al. (1999). Exact backscattering ($\xi = 0°$) occurs for $\psi - \psi' = 0°$, which agrees with the definition used for the GOME-2 data products.

A2 Li–Sparse geometric kernel

The Li–Sparse geometric scattering kernel (Li and Strahler, 1986) is defined as:

$$K_{\text{geo}} = O - \sec\theta^\star - \sec\theta_0^\star + \frac{1}{2}(1 + \cos\xi^\star)\sec\theta^\star\sec\theta_0^\star \, . \tag{A3}$$

The term O in Eq. (A3) and the starred angles $\theta^\star$, $\theta_0^\star$, and $\xi^\star$ are calculated using the following set of equations:

$$\theta^\star = \arctan\left(\frac{b}{r}\tan\theta\right) \, , \quad \theta_0^\star = \arctan\left(\frac{b}{r}\tan\theta_0\right) \, , \tag{A4}$$

$$\cos\xi^\star = \cos\theta^\star\cos\theta_0^\star + \sin\theta^\star\sin\theta_0^\star\cos(\psi - \psi') \, , \tag{A5}$$

$$O = \frac{1}{\pi}(t - \sin t\cos t)(\sec\theta^\star + \sec\theta_0^\star) \, , \tag{A6}$$

$$\cos t = \frac{h}{b}\frac{\sqrt{D^2 + (\tan\theta^\star\tan\theta_0^\star\sin(\psi - \psi_0))^2}}{\sec\theta^\star + \sec\theta_0^\star} \, , \tag{A7}$$

$$D = \sqrt{\tan^2\theta^\star + \tan^2\theta_0^\star - 2\tan\theta^\star\tan\theta_0^\star\cos(\psi - \psi')} \, . \tag{A8}$$

The parameters b/r and h/b are the crown relative shape and the crown relative height, respectively. These were fixed to 1 and 2, respectively, following Strahler et al. (1999).

References

75 Li, X. and Strahler, A. H.: Geometric-optical bidirectional reflectance modeling of a conifer forest canopy, IEEE Trans. Geosci. Remote Sens., GE-24, 906–919, https://doi.org/10.1109/TGRS.1986.289706, 1986.

Matthews, E.: Global vegetation and land use: New high-resolution data bases for climate studies, J. Clim. Appl. Meteor., 22, 474–487, https://doi.org/10.1175/1520-0450(1983)022<0474:GVALUN>2.0.CO;2, 1983.

Roujean, J.-L., Leroy, M., and Deschamps, P.-Y.: A bidirectional reflectance model of the Earth's surface for the correction of remote sensing
80 data, J. Geophys. Res., 97, 20455–20468, https://doi.org/10.1029/92JD01411, 1992.

Strahler, A. H, Lucht, W., Schaaf, C. B., Tsang, T., Gao, F., Li, X., Muller, J.-P., Lewis, P., and Barnsley, M. J.: MODIS BRDF/Albedo Product: Algorithm Theoretical Basis Document, MODIS Science Team, Issue 5.0, April, available at: https://modis.gsfc.nasa.gov/data/atbd/atbd_mod09.pdf, 1999.

Wanner, W., Li, X., and Strahler, A. H.: On the derivation of kernels for kernel-driven models of bidirectional reflectance, J. Geophys. Res.,
85 100, 21077–21089, https://doi.org/10.1029/95JD02371, 1995.